



Implications of High Polarization Degree for the Surface State of Ryugu

Daisuke Kuroda¹, Jooyeon Geem², Hiroshi Akitaya^{3,4}, Sunho Jin², Jun Takahashi⁵, Koki Takahashi⁶, Hiroyuki Naito⁷, Kana Makino⁸, Tomohiko Sekiguchi⁶, Yoonsoo P. Bach², Jinguik Seo², Shuji Sato⁹, Hiroshi Sasago¹⁰, Koji S. Kawabata⁴, Aoi Kawakami⁵, Miyako Tozuka⁵, Makoto Watanabe¹¹, Seiko Takagi¹², Kiyoshi Kuramoto¹², Makoto Yoshikawa¹³, Sunao Hasegawa¹³, and Masateru Ishiguro²

¹ Okayama Observatory, Kyoto University, 3037-5 Honjo, Kamogata-cho, Asakuchi, Okayama 719-0232, Japan; dikuroda@kwasan.kyoto-u.ac.jp

² Department of Physics and Astronomy, Seoul National University, Gwanak-gu, Seoul 08826, Republic of Korea

³ Planetary Exploration Research Center, Chiba Institute of Technology, Tsudanuma, Narashino, Chiba 275-0016, Japan

⁴ Hiroshima Astrophysical Science Center, Hiroshima University, Higashihiroshima, Hiroshima 739-8526, Japan

⁵ Nishi-Harima Astronomical Observatory, Center for Astronomy, University of Hyogo, Sayo, Hyogo 679-5313, Japan

⁶ Asahikawa Campus, Hokkaido University of Education, Hokumon, Asahikawa, Hokkaido 070-8621, Japan

⁷ Nayoro Observatory, Nisshin, Nayoro, Hokkaido 096-0066, Japan

⁸ Nayoro City University, Nishi 4-jo, Nayoro, Hokkaido 096-8641, Japan

⁹ Astrophysics Department, Nagoya University, Chikusa-ku, Nagoya, Aichi, 464-8602, Japan

¹⁰ Sasago Co.,Ltd., Chikusa-ku Nagoya, Aichi, 464-0815, Japan

¹¹ Department of Applied Physics, Okayama University of Science, Kita-ku, Okayama, Okayama 700-0005, Japan

¹² Department of CosmoSciences, Hokkaido University, Kita-ku, Sapporo, Hokkaido 060-0810, Japan

¹³ Institute of Space and Astronautical Science, Japan Aerospace Exploration Agency, Sagami-hara, Kanagawa 252-5210, Japan

Received 2021 January 21; revised 2021 February 27; accepted 2021 March 12; published 2021 April 20

Abstract

The asteroid exploration project “Hayabusa2” has successfully returned samples from the asteroid (162173) Ryugu. In this study, we measured the linear polarization degrees of Ryugu using four ground-based telescopes from 2020 September 27 to December 25, covering a wide-phase angle (Sun-target-observer’s angle) range from 28° to 104°. We found that the polarization degree of Ryugu reached 53% around a phase angle of 100°, the highest value among all asteroids and comets thus far reported. The high polarization degree of Ryugu can be attributed to the scattering properties of its surface layers, in particular the relatively small contribution of multiply scattered light. Our polarimetric results indicate that Ryugu’s surface is covered with large grains. On the basis of a comparison with polarimetric measurements of pulverized meteorites, we can infer the presence of submillimeter-sized grains on the surface layer of Ryugu. We also conjecture that this size boundary represents the grains that compose the aggregate. It is likely that a very brittle structure has been lost in the recovered samples, although they may hold a record of its evolution. Our data will be invaluable for future experiments aimed at reproducing the surface structure of Ryugu.

Unified Astronomy Thesaurus concepts: Near-Earth objects (1092); Asteroids (72)

1. Introduction

The Hayabusa2 spacecraft landed on the target C-type asteroid (162173) Ryugu and successfully collected surface materials in its sample-returning mission. This is the world’s first successful attempt to acquire the surface materials from a C-type asteroid that may contain organic compounds and hydrated minerals (Burbine et al. 2008). This sample was just returned to Earth on 2020 December 6. The new close-up images of Ryugu have raised a new question. Conventionally, it is considered that the surfaces of airless solar system bodies are covered with small dust grains (so-called regolith). Most of these small grains are the products of past impacts with other celestial bodies. It is also known that the temperature difference between day and night generates mechanical stress and breaks up large surface boulders to produce these small dust grains, a process known as thermal fatigue (Delbo et al. 2014).

However, from the new high-resolution images, it can be seen that the surface of Ryugu is covered with large lumpy stones without noticeably smaller particles (Jaumann et al. 2019; Sugita et al. 2019). There are many cobble-sized rocks but no pebble- or sand-sized particles ($\lesssim 1$ cm). This fact raises a question as to where the small grains produced by impacts and thermal fatigue have gone. It may be that the surface rocks

are covered with small adhesive grains, and Hayabusa2’s cameras could not resolve such small particles because of insufficient resolution, as suggested in Morota et al. (2020). Further observational data will be required to follow-up on the insufficient resolution of the onboard instruments.

Polarimetry is a powerful tool for investigating the sub-microscopic structures of surficial materials (Geake & Dollfus 1986). The linear polarization degree P_r of solar system objects is conventionally defined as $P_r = (I_N - I_P)/(I_N + I_P)$, where I_N and I_P are the intensities polarized in directions perpendicular to and parallel to the scattering plane, respectively. P_r depends on the phase angle (Sun-target-observer’s angle, α), with a negative branch indicated by low phase angles ($\alpha \lesssim 20^\circ$) and a positive branch at larger phase angles ($\alpha > 20^\circ$) with a maximum value P_{\max} of approximately $\alpha = 100^\circ$.

So far, there has been no polarimetric measurement of Ryugu. Here we provide the first polarimetric data on Ryugu, measured at four different observatories. Because of observational circumstances during late 2020, our data cover only the positive branch of P_r . For this reason, we mostly focus on the derivation of P_{\max} in this paper. We introduce our observations and data analysis in Section 2, show our findings in Section 3, and discuss the results in Section 4.

Table 1
List of Telescopes and Observational Instruments

Observatory Oper. Org. ^c	Telescope ^a Aperture	Instrument ^b Reference	Camera/Sensor Active Pixels	Pixel Scale Pixel Size	Polarizer
Hokkaido University Hokkaido Univ.	Pirka 1.6 m	MSI Watanabe et al. (2012)	Hamamatsu C9100-13 512 × 512	0''389 pixel ⁻¹ 16 μm	Wollaston
Higashi-Hiroshima Hiroshima Univ.	Kanata 1.5 m	HONIR Akitaya et al. (2014)	Hamamatsu 2k × 4k ^d 2048 × 4096	0''294 pixel ⁻¹ 15 μm	Wollaston
Nishi-Harima Univ. of Hyogo	Nayuta 2.0 m	WFGS2 Uehara et al. (2004)	FLI ^e PL230-42 2048 × 2048	0''198 pixel ⁻¹ 15 μm	Wollaston
Bohyunsan KASI ^g	 1.8 m	TRIPOL #3 Sato et al. (2019)	SBIG ^f ST-9XEi 512 × 512	0''29 pixel ⁻¹ 20 μm	Wire-grid

Notes.

^a Telescope nickname, if any.

^b Abbreviation of the instrument used.

^c Operational organization.

^d Hamamatsu Photonics fully depleted back-illuminated CCD.

^e Finger Lakes Instrumentation.

^f Santa Barbara Instrument Group.

^g Korea Astronomy and Space Science Institute.

2. Observations and Data Analysis

We observed the linear polarization degree of the near-Earth asteroid (NEA) (162173) Ryugu using the polarization modes of four telescopes and their respective mounted instruments: the Multi-Spectral Imager (MSI; Watanabe et al. 2012) using the 1.6 m Pirka telescope at the Hokkaido University Observatory, the Hiroshima Optical and Near-Infrared camera (HONIR; Akitaya et al. 2014) using the 1.5 m Kanata telescope at the Higashi-Hiroshima Observatory, the Wide Field Grism Spectrograph 2 (WFGS2; Uehara et al. 2004) using the 2.0 m Nayuta telescope at the Nishi-Harima Astronomical Observatory, and the Triple Range Imager and POLarimeter #3 (hereafter, TRIPOL; Sato et al. 2019) using the 1.8 m telescope at the Bohyunsan Optical Astronomy Observatory. Each instrument, mounted at Cassegrain focus, is designed to obtain highly accurate and reliable polarimetric data by rotating a half-wave plate against a fixed polarizer. Detailed information on the observational instruments is summarized in Table 1. The HONIR has simultaneous polarization imaging abilities in the visible and near-infrared regions, whereas three visible bands are available for TRIPOL. Only the R_C band was used in this study.

The methods for processing the data here were similar to those used in our previous studies (Ishiguro et al. 2017; Kuroda et al. 2018, 2021), and we thus omit a detailed description. After instrument-specific image processing (i.e., bias/dark subtraction, flat correction, and cosmic-ray removal), we conducted aperture photometry (typically using about 3–4 times the FWHM of the point source as the aperture diameter) of ordinary and extraordinary light on one frame. For TRIPOL without a beam-splitting prism, one light source was measured per frame. We noticed that the TRIPOL half-wave plate sometimes did not rotate properly, indicating an unusual signal level of the sky background (because the sky is highly polarized). We examined the background light values and excluded such data for the following analysis. We calculated the Stokes parameters for a set of four angles of the half-wave plate (0°, 45°, 22°5, and 67°5) and derived the linear polarization degree from these (Tinbergen 1996). From the multiple sets taken on the same night (i.e., the N columns in Table 1), we computed a weighted average. The values

regarding the linear polarization degree and position angle of polarization for Ryugu are summarized in Table 2, including information on the date of observation, the phase angle, and other parameters. Our data reduction was performed by combining Image Reduction and Analysis Facility (IRAF; Tody 1993) and our own script. The data obtained at each site were corrected for instrumental polarization with unpolarized stars and for the celestial plane with strongly polarized stars (Turnshek et al. 1990; Schmidt et al. 1992). We also observed the same polarization standard star BD+59d389 (Schmidt et al. 1992) and checked the consistency of the data obtained at all four sites.

3. Results

From 2020 September to December, we obtained polarimetric data for Ryugu at 23 nights in the R_C band and 1 night in the V band, with phase angles ranging from 28° to 104°. Figure 1 plots the nightly weighted average of the linear polarization degrees for Ryugu versus the phase angle, as well as a corresponding fitting curve. It was found that there was a clear change in the degree of polarization depending on the phase angle. According to our observations, the maximum polarization degree (P_{\max}) of Ryugu reaches $\gtrsim 53\%$. Because it was not yet decreasing at this value, the peak may even be a few percent higher than the observed maximum value. We applied the Lumme and Muinonen function (Lumme & Muinonen 1993; Penttilä et al. 2005) for this curve fitting, defined as

$$P(\alpha) = b(\sin \alpha)^{c_1} (\cos(0.5\alpha))^{c_2} \sin(\alpha - \alpha_0), \quad (1)$$

where b , c_1 , c_2 , and α_0 denote positive constants. Although this Equation (1) is an empirical function and may not always simulate the phase angle–polarization degree, the fitting results obtained via both the Markov Chain Monte Carlo (MCMC) and nonlinear least squares (NLS) methods (Levenberg–Marquardt (L-M) algorithm) yielded similar values. The expected maximum values were $P_{\max} = 53.0\%_{-1.5\%}^{+1.9\%}$, with the phase angle in this case being $\alpha_{\max} = 101.7^{\circ}_{-4.8}^{+8.4}$ (MCMC), and $P_{\max} = 53.3\%_{-5.1\%}^{+5.9\%}$, with $\alpha_{\max} = 102.2^{\circ}_{-17.7}^{+19.3}$ (L-M). Because no small phase angle data are available for this asteroid, we

Table 2
Summaries of Polarimetric Results for Ryugu

Date	Filter ^a	Exp ^b (s)	N^c	α^d ($^\circ$)	$P \pm \sigma P^e$ (%)	$\theta_p \pm \sigma \theta_p^f$ ($^\circ$)	$P_r \pm \sigma P_r^g$ (%)	$\theta_r \pm \sigma \theta_r^h$ ($^\circ$)	Inst. ⁱ
2020 Sep 27	R_C	120	12	28.27	3.60 ± 0.68	77.90 ± 5.40	3.59 ± 0.68	2.05 ± 5.40	HONIR
2020 Oct 09	R_C	60, 120	1, 4	31.40	6.29 ± 1.29	-13.13 ± 4.79	6.25 ± 1.29	3.15 ± 4.79	MSI
2020 Oct 10	R_C	120	3	31.89	4.19 ± 0.78	-19.12 ± 4.49	4.17 ± 0.78	-2.84 ± 4.49	MSI
2020 Oct 13	V	300	6	33.57	7.13 ± 0.33	36.07 ± 1.32	7.12 ± 0.33	-1.29 ± 1.32	WFGS2
2020 Oct 18	R_C	120	12	36.79	8.53 ± 0.31	-19.36 ± 1.03	8.48 ± 0.31	-3.08 ± 1.03	MSI
2020 Oct 19	R_C	120	2	37.61	10.41 ± 0.75	17.06 ± 2.07	10.29 ± 0.75	-4.35 ± 2.07	HONIR
2020 Nov 06	R_C	60, 90	1, 1	53.48	27.65 ± 6.98	-34.35 ± 5.72	22.33 ± 6.98	-18.07 ± 5.72	MSI
2020 Nov 09	R_C	120	12	56.43	22.82 ± 0.52	-10.22 ± 0.66	22.79 ± 0.52	-1.60 ± 0.66	HONIR
2020 Nov 11	R_C	120	3	58.33	23.10 ± 1.79	-18.46 ± 2.12	23.03 ± 1.79	-2.18 ± 2.12	MSI
2020 Nov 15	R_C	180, 300	2, 4	62.62	28.18 ± 0.16	-15.87 ± 0.22	28.11 ± 0.16	2.05 ± 0.22	WFGS2
2020 Nov 30	R_C	60, 120	4, 6	78.50	44.55 ± 1.16	-24.05 ± 0.74	44.37 ± 1.16	-2.53 ± 0.74	TRIPOL
2020 Dec 02	R_C	90	22	80.71	45.69 ± 1.29	-24.01 ± 0.81	45.58 ± 1.29	-1.99 ± 0.81	TRIPOL
2020 Dec 04	R_C	90	5	82.94	45.79 ± 2.41	-24.73 ± 1.50	45.64 ± 2.41	-2.34 ± 1.50	TRIPOL
2020 Dec 05	R_C	120	13	84.09	47.47 ± 0.62	-23.94 ± 0.38	47.41 ± 0.62	-1.41 ± 0.38	HONIR
2020 Dec 05	R_C	180	3	84.18	47.35 ± 0.82	-24.46 ± 0.45	47.24 ± 0.82	1.92 ± 0.45	WFGS2
2020 Dec 06	R_C	90	11	85.17	48.70 ± 1.07	-25.20 ± 0.63	48.51 ± 1.07	-2.58 ± 0.63	TRIPOL
2020 Dec 08	R_C	90	22	87.49	49.02 ± 1.19	-23.36 ± 0.70	49.00 ± 1.19	-0.66 ± 0.70	TRIPOL
2020 Dec 09	R_C	90	24	88.62	50.98 ± 1.06	-25.06 ± 0.60	50.81 ± 1.06	-2.37 ± 0.60	TRIPOL
2020 Dec 10	R_C	90	4	89.68	50.88 ± 2.54	-25.55 ± 1.43	50.62 ± 2.54	-2.93 ± 1.43	TRIPOL
2020 Dec 13	R_C	180	6	93.10	53.41 ± 0.62	-23.92 ± 0.31	53.31 ± 0.62	1.75 ± 0.31	WFGS2
2020 Dec 13	R_C	120	12	93.13	52.60 ± 1.46	-24.39 ± 0.80	52.44 ± 1.46	-2.23 ± 0.80	HONIR
2020 Dec 15	R_C	120	9	95.29	52.28 ± 1.73	-25.00 ± 0.95	51.92 ± 1.73	-3.57 ± 0.95	HONIR
2020 Dec 16	R_C	120	3	96.40	54.12 ± 2.07	-24.85 ± 1.09	53.71 ± 2.07	-3.83 ± 1.09	HONIR
2020 Dec 17	R_C	120	11	97.44	53.08 ± 1.14	-24.19 ± 0.62	52.73 ± 1.14	-3.29 ± 0.62	HONIR
2020 Dec 19	R_C	120	5	99.47	53.62 ± 2.55	-23.70 ± 1.36	53.17 ± 2.55	-3.73 ± 2.55	HONIR
2020 Dec 25	R_C	120	2	104.38	56.14 ± 8.26	-21.77 ± 4.22	55.11 ± 8.26	-5.49 ± 4.22	HONIR

Notes.^a Employed filters.^b Typical exposure time per frame in seconds.^c Number of sets counted as one in the four directions of the half-wave plate.^d Median phase angle (Sun–Ryugu–Observer angle) in degree.^e Degree of linear polarization in percent.^f Position angle of the polarization (in degrees equatorial E of N).^g Degree of linear polarization with respect to the scattering plane in percent.^h Position angle of the polarization with respect to the normal to the scattering plane (measured counterclockwise as viewed by the observer, in degrees)ⁱ Abbreviation of the instrument used.

refrain from mentioning any polarization parameters at low α values (i.e., the minimum value of the polarization degree (P_{\min}), inversion angle (α_0), and polarimetric slope (h)), which is beyond the scope of this work.

Figure 2 compares the phase angle–polarization degree variations in Ryugu, other asteroids, and cometary nucleus. The polarization degree of Ryugu is equal to or even greater than that of (3200) Phaethon (Ito et al. 2018), which is known to be the highest yet observed. In terms of cometary nucleus, it is also clearly higher than the reported values of $\sim 30\%$ for 209P/LINEAR (Kuroda et al. 2015). The phase angle dependence of the polarization degrees for Ryugu is similar to that of (152679) 1998 KU₂ (Kuroda et al. 2018), whereas it slightly differs from that of (101955) Bennu (Cellino et al. 2018), which is the target of the OSIRIS-REx mission. Spectroscopically, Ryugu is classified as a C(Bus-DeMeo¹⁴)- or Cb(Bus¹⁵)-type asteroid (Moskovitz et al. 2013; Tatsumi et al. 2020), and 1998 KU₂ is also Cb(Bus²)-type (Binzel et al. 2004). The geometric albedo

of Ryugu is slightly brighter, at 0.04–0.045 (Sugita et al. 2019; Tatsumi et al. 2020), than that of 1998 KU₂, at 0.018–0.03 (Mainzer et al. 2011; Nugent et al. 2016). However, considering the dependability of the absolute magnitude (H_{mag}) used to calculate the albedo of 1998 KU₂ (Masiero et al. 2021), this mismatch is probably within the margin of error. Therefore, we can conclude that Ryugu and 1998 KU₂ have very similar polarimetric and spectroscopic features.

4. Discussion

Ryugu has the highest degree of polarization in any airless solar system object previously observed. Because the polarization degree is determined by the surface conditions, there exists a mechanism that produces a high polarization degree on the surface layer of Ryugu. Umov law (Umov 1905), which is known as the inverse correlation between albedo and polarization, states that the darker the object, the higher the degree of polarization of the scattered light. The geometric albedo of Ryugu is very low, ranging from 0.04 to 0.045 (Sugita et al. 2019; Tatsumi et al. 2020). The light-scattering properties of such low albedo are consistent with a qualitatively higher degree of polarization because it inhibits multiple scattering (Bohren & Huffman 1998). Given the polarimetric measurements taken

¹⁴ Bus-DeMeo asteroid taxonomy classification based on visible and near-infrared spectroscopy (DeMeo et al. 2009).

¹⁵ Bus asteroid taxonomy classification based on visible spectroscopy (Bus & Binzel 2002).

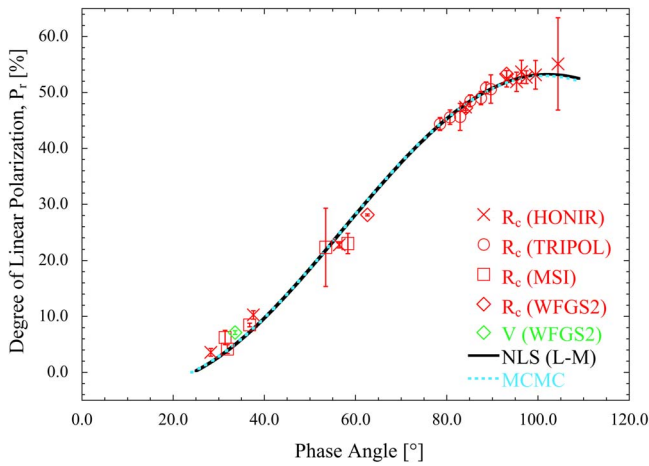


Figure 1. Linear polarization degree of Ryugu as a function of the phase angle. The data plotted are the weighted average (P_r) of each night shown in Table 2. Legend symbols were used separately for each instrument (i.e., crosses for HONIR, open circles for TRIPOL, open squares for MSI, and open diamonds for WFGS2). Red is used for the R_c band, and green for the V band. The solid black and dotted cyan lines denote the fitting models using the NLS method of the L-M algorithm and MCMC method for Equation (1), respectively. In both algorithms, the maximum polarization degree of Ryugu was estimated to be approximately 53%.

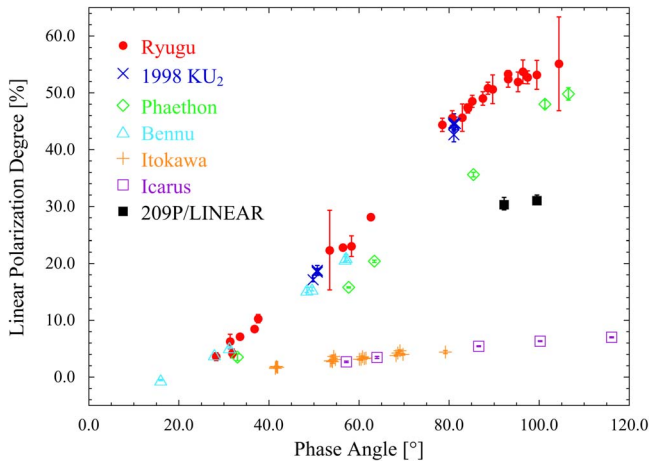


Figure 2. Phase angle–polarization dependence of NEAs and cometary nuclei in the red region. The solid red circles represent the polarimetric data for Ryugu. Data for the other NEAs include those from (152679) 1998 KU₂ (blue crosses; Kuroda et al. 2018), (3200) Phaethon (open green diamonds; Ito et al. 2018), (101955) Bennu (open cyan triangles; Cellino et al. 2018), (25143) Itokawa (orange pluses; Cellino et al. 2015), and (1566) Icarus (open purple squares; Ishiguro et al. 2017). The 209P/LINEAR (solid black squares; Kuroda et al. 2018) correspond to the polarization degree of the cometary nucleus subtracted its coma component. The linear polarization degree of Ryugu was found to reach the highest value among those measured in existing research.

using the returned samples of various shapes and sizes acquired by Hayabusa2, we expect to identify and quantify the physical quantities responsible for the polarization degree.

Although we recognize that the returned sample measurements will narrow down the physical property on Ryugu, as a leading study, we try to constrain the surface state from our polarization data. Generally, multiple scattering is generated by the repeated reflection and refraction of incident light inside an object and is often associated with dense materials. When focusing on the scattering frequency of a surface layer, it is predicted that a larger particle size per unit volume will lower the scattering frequency. Until now, polarimetric measurements

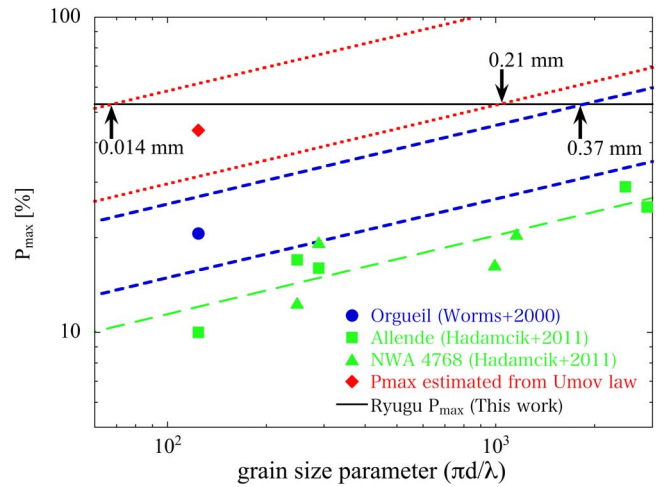


Figure 3. Grain size parameter vs. maximum value of the polarization degree (P_{\max}). The size parameter is a dimensionless quantity expressed by $\pi d/\lambda$, where d and λ represent the particle equivalent diameter and wavelength, respectively (Bohren & Huffman 1998). The solid green squares and solid green triangles denote two size-sorted carbonaceous chondrites, Allende and NWA 4768 meteorites, respectively (Hadamcik et al. 2011). The trend of increasing P_{\max} with grain size for these meteorites is shown by the long green dashed line. Assuming that this proportional relationship including its deviation holds for lower albedo, the range of low albedo (~ 0.06) is represented by the blue dashed lines and the range of very low albedo (0.032–0.034, converted from $p_v = 0.04$ –0.045 for Ryugu) by the red dotted lines. The solid blue circle indicates the pulverized Orgueil meteorite (20–30 μm), which is the low albedo carbonaceous meteorite (Worms et al. 2000). The solid red diamond is the reference point of the very low albedo, which has the same grain size of $\sim 25 \mu\text{m}$ and is estimated from Umov law (Umov 1905). From the intersection of this region and Ryugu's P_{\max} (solid black line), we estimated a grain size of 0.37 mm at the low limit for low albedo (~ 0.06) and 0.014–0.21 mm for very low albedo (0.032–0.034).

of meteorites (especially with low albedos) have been limited. Among them, the polarization degree of 20–30 μm aggregates of pulverized Orgueil meteorite, the primitive meteorite with low albedo (~ 0.06 at $\alpha = 6^\circ$, where α means the phase angle), was measured to have a maximum value $P_{\max} = 20.6\%$ at 638 nm under the deposited condition (Worms et al. 2000). Polarimetric measurements using slightly brighter meteorites indicated that P_{\max} was approximately three times higher when the grain size increased from $<25 \mu\text{m}$ to $<500 \mu\text{m}$ for Allende, and approximately 1.3 times higher when the grain size increased from $<50 \mu\text{m}$ to $<200 \mu\text{m}$ for NWA 4768 (Hadamcik et al. 2011). That is, as the particle size increases in this size range, the degree of polarization tends to be higher. Applying the relationship between particle size and polarization degree to the lower albedo meteorite (i.e., Orgueil), coupled with the P_{\max} derived in this study, we obtain the particle size boundary. The bounds of the particle size represent a range that takes into account the error of the applied slope and depends on the data variances of Allende and NWA 4768. We derived a lower limit size of 0.37 mm, but avoided specifying the upper limit, because for some materials, the polarization degree reaches a plateau with increasing size parameter (Hadamcik et al. 2009), and there were concerns about extrapolation to larger size parameters (Figure 3). This lower limit estimate is consistent with the 0.2–2 mm (the square roots of 0.03–4.56 mm^2) bright inclusions identified in proximate images of Ryugu (Jaumann et al. 2019). Considering that the very low albedo of Ryugu ($p_v = 0.04$ –0.045) is due to the dark matrix, we attempted to derive a polarimetrically dominant

grain size for Ryugu. The albedo of Ryugu at $\alpha = 6^\circ$, which is adjusted to the measurement conditions of the meteorites, is 0.032–0.034 (Tatsumi et al. 2020). The Ryugu-equivalent reference point (red diamond symbol) shown in Figure 3 was calculated from Umov law using the P_{\max} and albedos of Allende (~ 0.11 for $<25 \mu\text{m}$) and Orgueil (~ 0.06 for $20\text{--}30 \mu\text{m}$) meteorites. If the above relationship between particle size and polarization degree applies to the very low albedo asteroid (i.e., 0.032–0.034 for Ryugu), we also infer that submillimeter order particles are dominant in the surface layer of Ryugu. In meteorites, the matrix grain size is generally finer than the inclusions, which is qualitatively consistent with our derivation.

On the other hand, the observational results of an optical navigation camera (ONC-T), a radiometer (MARA), and a camera (MasCam) on board the mobile asteroid surface scout (MASCOT) of Hayabusa2 reported that the surface layer of Ryugu was covered with submeter- to meter-sized rocks, with no fine-grain dust below the millimeter order (Grott et al. 2019; Jaumann et al. 2019; Sugita et al. 2019). On the basis of the result of a thermal infrared imager (TIR), the rocks of the Ryugu surface are much more porous than typical carbonaceous chondrite meteorites, and the surrounding soils are similarly porous and covered with small pieces of rock >10 cm in diameter (Okada et al. 2020). By regarding it as a thermally consolidated block, the size of the domain particles that comprise the rock is not constrained. Data from thermal infrared observations indicate that the surface layer of Ryugu has a very high porosity (Grott et al. 2019; Ogawa et al. 2019; Shimaki et al. 2020). Thus we also consider that our estimate (i.e., submillimeter-sized grains) corresponds to particle sizes that constitute highly porous aggregates, whose agglomerates form centimeter to submeter rocks. A possible interpretation of the size (determined by our polarimetry) is that the cauliflower-like structures on the rock appearances observed by MASCOT are attributed to determining the polarimetric property.

Although we acknowledge that our size estimate is crude because of the unavailability of polarimetric measurements of very dark meteorites, it seems that very small (micron-sized) grains are not so abundant as to reduce the P_{\max} . It is likely that the paucity of micron-sized particles may have been selectively ejected by some mechanisms such as levitation (Hartzell 2019), or may have been buried underground (Arakawa et al. 2020) or have been incorporated into larger grains during aggregate formation (Seiphoori et al. 2020). The most important contribution of this research is to provide basic polarimetric data for reproducing the physical conditions of the Ryugu surface layer. Further polarimetric investigation using Ryugu samples will specify the surface physical conditions.

5. Summary

We conducted polarimetric observations of the NEA (162173) Ryugu, which was thoroughly investigated by the Hayabusa2 spacecraft, from 2020 September to December. The degree of linear polarization of Ryugu was obtained for 24 nights over phase angles of $28^\circ\text{--}104^\circ$, and the following findings were obtained.

1. The polarization degree of Ryugu, which reached $\gtrsim 53\%$, is the highest ever recorded, exceeding that of Phaethon.
2. Submillimeter order grains are dominant in the surface layer of Ryugu, as inferred from comparison with polarimetric measurements of meteorites.

3. The results of in situ observations (MARA, MasCam, ONC-T, and TIR) of Hayabusa2, also indicate that this grain size reflects the constituents of larger aggregates.








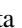






This study provides basic data that allows tracing of the brittle and fragile surface layers of Ryugu in the future.

We appreciate the anonymous referee for the careful reading of our manuscript and for providing helpful comments. M.I. was supported by the NRF funded by the Korean Government (MEST) grant No. 2018R1D1A1A09084105 and the Seoul National University Research Grant in 2018. The work of S.H. was supported by JSPS KAKENHI (grant Nos. JP18K03723, JP19H00719, and JP20K04055) and the Hypervelocity Impact Facility (former facility name: the Space Plasma Laboratory), ISAS, JAXA. S.J. was supported by the Global Ph.D. Fellowship Program through a National Research Foundation of Korea (NRF) grant funded by the Korean Government (NRF-2019H1A2A1074796). D.K. was funded by the Kyoto University Foundation. This research was partially supported by the Optical & Near-Infrared Astronomy Inter-University Cooperation Program, MEXT, of Japan. Our observation at the Bohyunsan Optical Astronomy Observatory was realized with the help of the observatory staff, especially Dr. Hyun-il Sung. We would like to thank the staff of the Nayoro Observatory for their cooperation in organizing our observation.

Facilities: Kanata:1.5 m, Nayuta:2.0 m, Pirka:1.6 m, BAAO:1.8m.

Software: astropy (Astropy Collaboration et al. 2013), IRAF (Tody 1993), SExtractor (Bertin & Arnouts 1996), SEP (Barbary 2016), PyMC3 (Salvatier et al. 2016).

ORCID iDs

Daisuke Kuroda  <https://orcid.org/0000-0002-7363-187X>
 Jooyeon Geem  <https://orcid.org/0000-0002-3291-4056>
 Hiroshi Akitaya  <https://orcid.org/0000-0001-6156-238X>
 Sunho Jin  <https://orcid.org/0000-0002-0460-7550>
 Hiroyuki Naito  <https://orcid.org/0000-0001-9067-7653>
 Tomohiko Sekiguchi  <https://orcid.org/0000-0003-1726-6158>
 Yoonsoo P. Bach  <https://orcid.org/0000-0002-2618-1124>
 Koji S. Kawabata  <https://orcid.org/0000-0001-6099-9539>
 Makoto Watanabe  <https://orcid.org/0000-0002-3656-4081>
 Seiko Takagi  <https://orcid.org/0000-0002-7084-0860>
 Kiyoshi Kuramoto  <https://orcid.org/0000-0002-6757-8064>
 Makoto Yoshikawa  <https://orcid.org/0000-0002-3118-7475>
 Sunao Hasegawa  <https://orcid.org/0000-0001-6366-2608>
 Masateru Ishiguro  <https://orcid.org/0000-0002-7332-2479>

References

- Akitaya, H., Moritani, Y., Ui, T., et al. 2014, *Proc. SPIE*, 9147, 914740
 Arakawa, M., Saiki, T., Wada, K., et al. 2020, *Sci*, 368, 67
 Astropy Collaboration, Robitaille, T. P., Tollerud, E. J., et al. 2013, *A&A*, 558, A33
 Barbary, K. 2016, *JOSS*, 1, 58
 Bertin, E., & Arnouts, S. 1996, *A&AS*, 117, 393
 Binzel, R. P., Rivkin, A. S., Stuart, J. S., et al. 2004, *Icar*, 170, 259
 Bohren, C. F., & Huffman, D. R. 1998, *Absorption and Scattering of Light by Small Particles* (Weinheim: Wiley-VCH Verlag GmbH & Co. KGaA)
 Burbine, T. H., Rivkin, A. S., Noble, S. K., et al. 2008, *RvMG*, 68, 273
 Bus, S. J., & Binzel, R. P. 2002, *Icar*, 158, 146
 Cellino, A., Bagnulo, S., Belskaya, I. N., & Christou, A. A. 2018, *MNRAS*, 481, L49

- Cellino, A., Gil-Hutton, R., & Belskaya, I. N. 2015, in *Polarimetry of Stars and Planetary Systems*, ed. L. Kolokolova, J. Hough, & A. Levasseur-Regourd (Cambridge: Cambridge Univ. Press), 360
- Delbo, M., Libourel, G., Wilkerson, J., et al. 2014, *Natur*, 508, 233
- DeMeo, F. E., Binzel, R. P., Slivan, S. M., & Bus, S. J. 2009, *Icar*, 202, 160
- Geake, J. E., & Dollfus, A. 1986, *MNRAS*, 218, 75
- Grott, M., Knollenberg, J., Hamm, M., et al. 2019, *NatAs*, 3, 971
- Hadamcik, E., Levasseur-Regourd, A. C., Renard, J. B., Lasue, J., & Sen, A. K. 2011, *JQSRT*, 112, 1881
- Hadamcik, E., Renard, J. B., Levasseur-Regourd, A. C., et al. 2009, *JQSRT*, 110, 1755
- Hartzell, C. M. 2019, *Icar*, 333, 234
- Ishiguro, M., Kuroda, D., Watanabe, M., et al. 2017, *AJ*, 154, 180
- Ito, T., Ishiguro, M., Arai, T., et al. 2018, *NatCo*, 9, 2486
- Jaumann, R., Schmitz, N., Ho, T.-M., et al. 2019, *Sci*, 365, 817
- Kuroda, D., Ishiguro, M., Naito, H., et al. 2021, *A&A*, 646, A51
- Kuroda, D., Ishiguro, M., Watanabe, M., et al. 2015, *ApJ*, 814, 156
- Kuroda, D., Ishiguro, M., Watanabe, M., et al. 2018, *A&A*, 611, A31
- Lumme, K., & Muinonen, K. O. 1993, IAU Symp. 160, *Asteroids, Comets, Meteors* (Houston, TX: LPI), 194
- Mainzer, A., Grav, T., Bauer, J., et al. 2011, *ApJ*, 743, 156
- Masiero, J. R., Wright, E. L., & Mainzer, A. K. 2021, *PSJ*, 2, 32
- Morota, T., Sugita, S., Cho, Y., et al. 2020, *Sci*, 368, 654
- Moskovitz, N. A., Abe, S., Pan, K.-S., et al. 2013, *Icar*, 224, 24
- Nugent, C. R., Mainzer, A., Bauer, J., et al. 2016, *AJ*, 152, 63
- Ogawa, K., Hamm, M., Grott, M., et al. 2019, *Icar*, 333, 318
- Okada, T., Fukuhara, T., Tanaka, S., et al. 2020, *Natur*, 579, 518
- Penttilä, A., Lumme, K., Hadamcik, E., & Levasseur-Regourd, A. C. 2005, *A&A*, 432, 1081
- Salvatier, J., Wiecki, T. V., & Fonnesbeck, C. 2016, PyMC3: Python probabilistic programming framework, Astrophysics Source Code Library, record ascl:1610.016
- Sato, S., Chieh Huang, P., Chen, W. P., et al. 2019, *RAA*, 19, 136
- Schmidt, G. D., Elston, R., & Lupie, O. L. 1992, *AJ*, 104, 1563
- Seiphoori, A., Ma, X.-g., Arratia, P. E., & Jerolmack, D. J. 2020, *PNAS*, 117, 3375
- Shimaki, Y., Senshu, H., Sakatani, N., et al. 2020, *Icar*, 348, 113835
- Sugita, S., Honda, R., Morota, T., et al. 2019, *Sci*, 364, 252
- Tatsumi, E., Domingue, D., Schröder, S., et al. 2020, *A&A*, 639, A83
- Tinbergen, J. 1996, *Astronomical Polarimetry* (Cambridge: Cambridge Univ. Press), 174
- Tody, D. 1993, in ASP Conf. Ser., 52, *Astronomical Data Analysis Software and Systems II*, ed. R. J. Hanisch, R. J. V. Brissenden, & J. Barnes (San Francisco, CA: ASP), 173
- Turnshek, D. A., Bohlin, R. C., Williamson, R. L. I., et al. 1990, *AJ*, 99, 1243
- Uehara, M., Nagashima, C., Sugitani, K., et al. 2004, *Proc. SPIE*, 5492, 661
- Umov, N. 1905, *PhyZ*, 6, 674
- Watanabe, M., Takahashi, Y., Sato, M., et al. 2012, *Proc. SPIE*, 8446, 84462O
- Worms, J.-C., Renard, J.-B., Hadamcik, E., Brun-Huret, N., & Levasseur-Regourd, A. C. 2000, *P&SS*, 48, 493